Tuning the Cu/SiO_2 wettability features for bio-derived platform molecules valorization

Denise Cavuoto, Nicoletta Ravasio, Federica Zaccheria, Marcello Marelli, Giuseppe Cappelletti*, Sebastiano Campisi, and Antonella Gervasini*

KEYWORDS

Hydrophobization, copper catalysts, hydrogenation, surface properties, bioalcohols.

ABSTRACT

A simple organosilane-grafting protocol has been used for the preparation of a copper heterogeneous catalyst with tunable wettability properties. A series of Cu/SiO_2 trietoxysilane-modified systems with gradually reduced alcolphilicity has been used in the hydrogenation of the platform molecule γ-valerolactone into 1,4-pentandiol, a valuable biobased monomer. The surface modification obtained with the proposed procedure allows to significantly increase the selectivity (99%) of the process and therefore the yield (80%) in the desired diol. Several characterization techniques (static contact angle, ATR, CP-MAS solid state NMR, pyridine and ammonia adsorption) put in light the modification of the surface while preserving the hydrogenation activity of the metallic phase. The results obtained show the opportunity given by this simple catalytic system in combining the activity of the copper phase and the modified polarity of the surface.

Introduction

The gradual substitution of petroleum resources with renewable biomasses for energy and chemical synthesis represents a crucial milestone on the roadmap towards environmental sustainability. Biomass is however, a very varied and complex feedstock that requires the challenging development of new processes for the production of biofuels[1] and biochemicals.[2–5] Moreover, with respect to the traditional fossil supplies, bio-based molecules can contain up to 50% wt of oxygen, mainly derived from -O-, -OH, -COOH and -COOR groups making them definitely more polar if compared to the petrol-based hydrocarbons. This fact requires important changes in the industrial processes and transformation procedures, obtaining also different final products.[6–9] For this reason, water or highly polar solvents are typically used for biomass transformations.

Heterogeneous catalysis has been widely studied in biomass valorization processes due to its versatility and agreement with the Green Chemistry principles,[10,11] as well as to its great success in traditional refinery processes. As known, the heterogeneous catalytic mechanism is a complex process involving several steps and including reagent adsorption and product desorption towards and from the catalyst surface. Based on these considerations, it is clear that working with of highly polar molecules that must interact with the surfaces of the catalyst makes phenomena such as surface wettability a key problem to be addressed in order to increase the reactivity of the catalysts.

The study of the surface properties of a catalyst, in particular the wettability, becomes mandatory in order to modulate the stability of the system on one hand and preferential adsorption or desorption of the organic biomass-derived molecules on the other.[12–15] In the recent literature, several examples are reported relying on the capacity of a more hydrophobic surface to boost catalyst resistance towards water, poisoning of the active sites, especially acidic ones, thus

allowing long-life and good recyclability of the system.[16–19] Therefore, a low hydrophilic surface is a good tool to improve dehydration of bio-based molecules (such as sorbitol to give isosorbide[20,21]), but also in the case of condensation like esterification of fatty acids[22–24] or biobased acids[25,26] and etherification.[27,28]

However, nowadays, there are few results regarding the hydrophobization of metal catalysts in the literature, that means related to the use of solids able to promote hydrogenation or oxidation reactions too. A viable strategy is the deposition or incorporation of metal particles onto a hydrophobic support matrix. Water resistant Pd on hierarchically porous zeolites, with different hydrophobic/hydrophilic character, were prepared demonstrating that modulating the wettability properties of the support affects the activity of the Pd active phase.[29] Otherwise, Pd can be incorporated on carbonaceous material with different hydrophobic degree for furfural and 5-(hydroxymethyl)-furfural hydrogenation in water. Also in this case, finely tuning of the support wettability can help to modulate the selectivity of the reaction achieving up to 99% selectivity towards tetrahydrofurfuryl alcohol.[30] Moreover, a electrochemical approach could be used to prepare Pt or Pd noble metal catalysts with wide range of wettability carefully tuning the deposition time.[31]

Another way to modulate wettability properties of metal catalysts is the post-synthesis modification of the surface.[32] An high water resistance and stability can be obtained by coating Ru/TiCeOx catalysts surface for o-dichlorobenzene catalytic combustion with phenyltriethoxysilane obtaining a superhydrophobic water repellant and self-cleaning material.[33] Many works had showed how surface modification of supported metal catalyst can drive the reaction pathway, boosting the selectivity towards a desired product. A series of organophosphonic acids can be used to tune the surface hydrophobicity of Pd/Al_2O_3 catalyst therefore allowing to

control the selectivity in vanillin hydrodeoxygenation reaction pathways.[34] Stearic acid functionalized Cu/ZnO exhibited a strong inhibitory effect on the unfavorable water–gas shift reaction in one-step synthesis of dimethyl ether from syngas.[35]

γ-Valerolactone (GVL) is a platform-molecule obtained from biomass lignocellulosic wastes and due to its versatility has been considered a benchmark key chemical in the biomass refinery.[36] In particular, GVL is the precursor of 1,4-pentanediol (1,4-PDO), a useful monomer of new renewable- or semi-renewable polyurethanes and polyesters synthesis.[37]

Trietoxyoctylsilane was utilized as a coupling agent for Cu catalyst in the hydrogenation of levulinic acid to give GVL. The obtained higher water repellency of the grafted materials not only boosted catalyst resistance but also GVL yield preventing the stabilization of the 4-hydroxyvaleric acid intermediate through intermolecular hydrogen bonds with water molecules.[38]

On the basis of these results, in the present work, we would like to demonstrate that a facile procedure of modification of the surface of a supported metal catalyst in the direction of increasing its lipophilic character through triethoxyoctylsilane (TEOCS) groups grafting is an effective tool to improve the catalytic performance in reactions concerning biomass. In particular, the influence of the lipophilicity of the surface of Cu/SiO_2 catalyst on the hydrogenation of GVL for the selective formation of 1,4-pentanediol is presented. Silylation has revealed to be a great tool for the hydrophobization of silica based materials.[39–41] The activity carried out was aimed at verifying that the triethoxyoctylsilane groups did not mask the copper sites at the surface making them less capable to interacting with the GVL and forming 1,4-PDO. For this reason, the quantity of grafted TEOCS groups has been modulated in a large interval (from 1 to 15% wt.%) generating some modified copper silica samples. Targeted characterization studies were aimed at verifying the

properties of the modified-silica surfaces differently rich in TEOCS groups in terms of wettability and acidity.

Experimental Section

Materials: SiO_2 (specific surface area of 410 m^2/g, total pore volume of 0.63 $cm^3\ g^{-1}$) was purchased by Fluka Chemicals. Highly pure (> 99%) trietoxyoctylsilane (TEOCS), γ-valero lactone (GVL) 1,4-pentanediol (1,4-PDO) and copper nitrate trihydrate were purchased from Sigma Aldrich. Cyclopentyl methyl ether (CPME), stabilized with butylated hydroxy toluene (purity > 99.5%), was purchased by Tokyo Chemical Industry.

Catalyst preparation: CuO/SiO_2 was prepared through a Chemisorption-Hydrolysis method[42] adding the silica support to an aqueous $[Cu(NH_3)_4]^{2+}$ solution, prepared by dropping NH_4OH to a $Cu(NO_3)_2\times 3H_2O$ solution the nominal copper loading of 16% and a pH of 9. After 20 min under stirring, the slurry was diluted with 3 L of water in an ice bath at 0 °C. Then, he solid was filtrated with a Büchner funnel, washed with water, dried overnight at 120 °C and calcined in air atmosphere at 350 °C for 4 h. The metal loading was confirmed by Inductively Coupled Plasma (ICP) analysis in our previous works.[43] The following code was used in the discussion of this paper: CuO in the case of calcined catalysts, Cu in the case of reduced catalyst slash the utilized support. Organosilane grafting was performed preparing a solution of TEOCS of the desired concentration (in the range 1%–15% w/w) in isopropanol in which 1 g of dry catalyst was dispersed. After 1 h of vigorous stirring at room temperature, the isopropanol was evaporated under vacuum at 50 °C.

Catalytic tests: Before any reaction the catalysts (100 mg) were pre-treated for 20 min at 270 °C under air and for 20 min under vacuum and then reduced through three hydrogen (1 bar) and vacuum cycles (5 mins each) at the same temperature. Generally, γ-valerolactone (5 mmol) was

dissolved in 20 mL of solvent. Then the pre-reduced catalyst was suspended in the reaction mixture and they were loaded under nitrogen flow in a 100 mL Parr reactor under different H_2 pressure (30–50 bar) and temperatures (140−180 °C) for 22 h under mechanical stirring (750 rpm). Reaction conversions and selectivity were determined by GC-FID analysis using an Agilent 6890 Gas 0,25 Chromatography system with a Alltech Heliflex AT-5 capillary column (30 m × 0.32 mm ID × 0.25 μm). Dodecane was used as internal standard (carbon balance >98%). Byproducts were qualitative determined with GCMS analysis using an Agilent 5957C GC–MS chromatograph with an HP-5 column. Conversion was determined using the following equation:

$$\% C = \frac{n(t_0) - n(t)}{n(t_0)} \times 100$$

where $n(t_0)$ are the initial moles of GVL introduced in the reactor and n(t) are the unreacted moles of GVL determined with GC-FID analysis. Selectivity was determined using this equation:

$$\% S = \frac{p(t)}{n(t_0) - n(t)} \times 100$$

where p(t) are the moles of products formed determined by GC-FID analysis. Byproducts were determined through GC-MS analysis.

Physico-chemical characterizations:

Solid state NMR spectra of the samples were obtained at 99.36 (^{29}Si) MHz on a Bruker Avance 500 spectrometer, equipped with a 4 mm magic angle spinning (MAS) broad-band probe (spinning rate νR up to 6 kHz). The MAS spectra were recorded on solid samples, typically around 150 mg. Each sample was packed into a 4-mm MAS rotor (50 μL sample volume) spinning at 6 kHz and at a temperature of 303 K with a contact time of 6 ms and accumulation time of 68 h; no resolution improvement was found at higher rate spinning and/or temperature. The experimental data were fitted by using a Gaussian function.[44]

Static contact angle (SCA) measurements of the tested solid supports were performed by means of a Krüss Easy instrument.[45] Notably, moulded thin disks (25-30 mg of the sample powders pressed at 3 tons) were prepared by using a Specac manual hydraulic press to achieve a compact and reasonably flat surface. A 1,3-propanediol drop of 5 μL was gently placed on the surface disk; the drop profile was extrapolated immediately after the contact with the surface, using a tangent fitting function to acquire the diol static contact angle (θ_{diol}). Measurements were repeated ten times to obtain a statistically relevant population.

Specific surface area (SSA) (determined by Brunauer Emmet Teller method) and pore volume (PV) (determined by using Barrett-Joyner-Halenda method) of the samples were measured after evacuation of the samples (ca. 0.2 g sieved as particles in the range of 80–200 mesh) at 200 °C for 6 h under vacuum by collecting N_2 adsorption/desorption isotherms at −196 °C using a Micromeritics ASAP 2020.

The water adsorption isotherms were collected on the same instrument and exploiting the same pre-treatment method of the samples adopted for the morphologic analyses above detailed. Adsorption of water was performed with 20 ml reservoir of ultrapure water as a vapor source and held at 40 °C. The adsorption experiments were carried out at 22 °C and the saturation pressure was 25 mmHg.

The Attenuated Total Reflection (ATR) spectra and Fourier Transform-Infrared (FT-IR) studies of the adsorption of the pyridine probe molecule were carried out on a FTS-60 spectrophotometer equipped with mid-IR MCT detector purchased from BioRad. The experiments were performed on a thin disk of sample (20–30 mg, pressed at 1–2 tons) after a reduction pre- treatment consisting in 20 min at 270° at air followed by 20 min at 270 °C under vacuum and finally a reduction under H_2 through three hydrogen (1 bar) and vacuum cycle at the same temperature. The first spectrum

was collected before pyridine adsorption as a blank. Then, pyridine vapors were adsorbed at room temperature and then desorbed in steps of 30 min until 250 °C at the given vacuum (10^{-5} bar). The spectrum of each desorption step was collected every 50 °C up to 250 °C. For quantitative analysis the amount of absorbed pyridine ($mmol_{py}\ g_{cat}^{-1}$) was calculated on the basis of the relationship reported by Emeis.[46]

Surface composition of all the samples was analyzed by X-ray Photoelectron Spectroscopy (XPS) by means of an M-PROBE Surface Spectrometer with an Al (Ka) source and a spot size from 0.15 mm to 1 mm in diameter. An applied voltage of 10 V and a vacuum of 10^{-8} –10^{-7} Torr were used. The survey scans were investigated in 0–1100 eV binding energy range, using a spot size of 800 μm with an energy resolution of 4 eV (scan rate of 1 eV per step). The samples were pre-treated with the same procedure of FT-IR analysis. ESCA Hawk Software was used for data curation.

Transmission electron microscopy (TEM): analysis was performed using a ZEISS LIBRA200FE. STEM (Scanning TEM) mode exploit a HAADF (High-angle annular dark-field) detector. The samples were gently smashed in an agate mortar, suspended in isopropyl alcohol for 20 min in an ultrasonic bath and dropped onto a lacey carbon-coated copper TEM grid. The samples were analyzed after complete solvent evaporation.

Total acidity of the bare CuO/SiO_2 and functionalized samples was determined by NH_3 adsorption under flowing dynamic experiments. The dried sample (ca. 0.15 g, 45–60 mesh) was activated at 150 °C under flowing nitrogen for 30 min in a glass tubular reactor; then, the NH_3/N_2 mixture (ca. 500 ppm of NH_3) flowed at 3 $NL{\cdot}h^{-1}$ through the sample maintained at 80°C and reached a gas cell (path length 2.4 m multiple reflection gas cell) in the beam of a Fourier Transform InfraRed spectrometer, FT-IR (equipped with a DTGS detector, Bio-Rad, Hercules,

CA, USA). The NH_3 stretching mode (966 cm^{-1}) was monitored as a function of time. The detailed adopted procedure and data computation were described elsewhere.[47]

Assuming a 1:1 stoichiometry for the NH_3 adsorption on the surface acid site, the amount of acid sites per sample mass (in $\mu mol \cdot g^{-1}$) was determined.

Mass loss of catalysts was determined by thermogravimetric analysis (TGA) on a TGA 7, Perkin Elmer analyzer, the experiments aimed at determining the stability of the silane groups. Prior to the analysis, the sample was stored in oven overnight. Then, a weighted amount of the saturated sample (ca. 10-15 mg) was loaded on the pan of the thermobalance. Each experiment was carried out under nitrogen flowing gas (60 mL min^{-1}). The thermal program comprised three steps: i) isothermal step at 50 °C for 10 min; ii) heating at rate 20 °C/min up to 700 °C[48]. The instrument accuracy is around few μg.

Results and discussion

The role of both wettability and acidity of the modified-silica surfaces is pivotal in influencing the final performances of the catalysts in the hydrogenation of GVL to give 1,4-PDO (Scheme 1), as already mentioned in our previous work.[49]

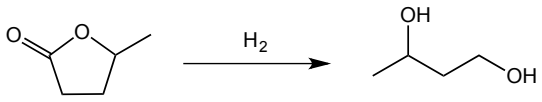

Scheme 1. Hydrogenation of GVL to obtain 1,4-PDO.

Particularly, CuO/SiO_2 catalyst prepared with the less hydrophilic surface achieved higher selectivity in the diol product when operating in the green cyclopentyl methyl ether (CPME) solvent. In this work the silica supported copper catalyst was prepared depositing the metal on silica gel with the Chemisorption-Hydrolysis method.[42] To modulate the wettability features of the

surface, triethoxyoctylsilane (TEOCS) groups were anchored to the surface hydroxyl groups at different silane percentage loadings (1%, 5%, 10% and 15% w/w). In order to investigate the effect of the silane surface density on the catalytic performances, the bare and the functionalized catalysts were tested in the hydrogenation reaction described in Scheme 1 under the reaction conditions already used and described in our the previous work.[49] In Figure 1, results obtained in the catalytic tests are showed.

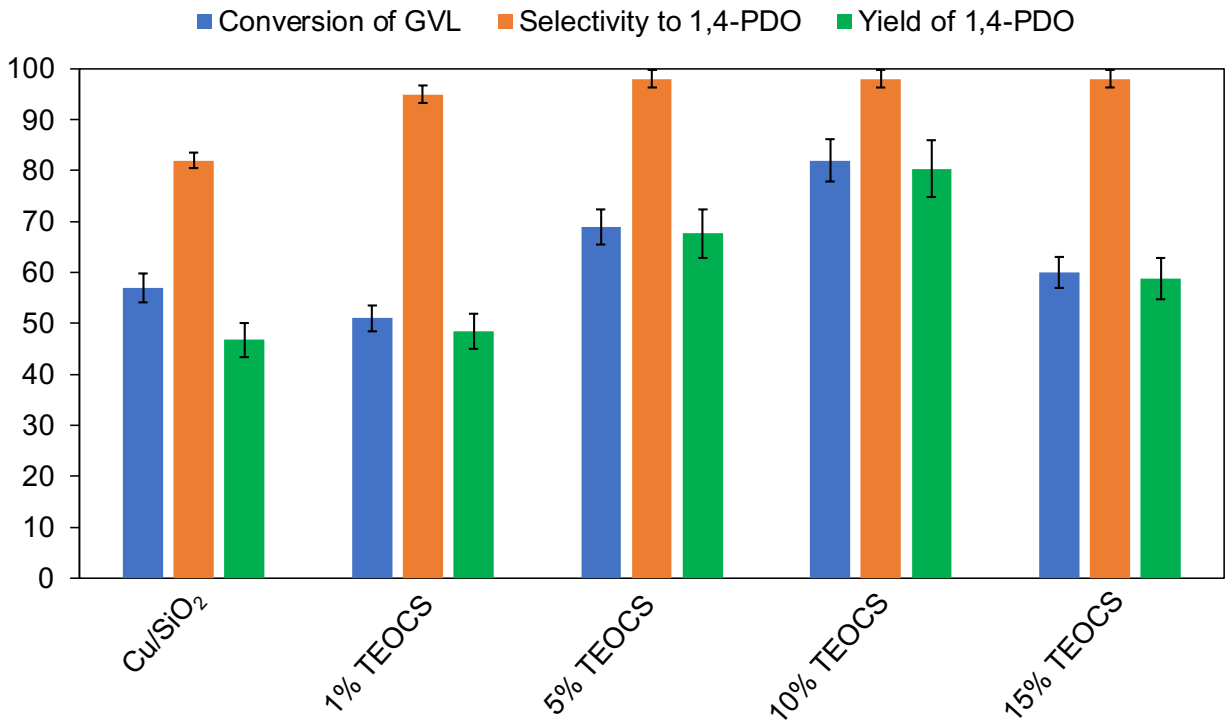

Figure 1. Catalytic test results of the prepared catalysts in the GVL hydrogenation. Reaction conditions: T = 160°C, P(H_2) = 50 bar, t = 22 h, substrate/catalyst = 5/1 and solvent: CPME.

After low addition (1% of loading) of the silane chains on Cu/SiO_2, we readily observed an increase in selectivity to 1,4-PDO. The overall activity improved too, raising from the 47% yield of 1,4-PDO obtained with the unfunctionalized Cu/SiO_2 to 80% yield observed with the Cu/SiO_2 - 10% TEOCS. Interestingly, a marked yield decrease is appreciable when increasing the

silane loading percentage more than 10%, *i.e.* 15%, while keeping an excellent selectivity toward the diol. In fact, conversely to what observed with the polar unfunctionalized Cu/SiO_2 catalyst, a more efficient desorption of 1,4-PDO strongly limits the formation of byproducts such as dehydration ones (methyl-tetrahydrofuran),[50] that is the same effect previously observed by using a less polar matrix as the support.[49]

To properly understand the effect of the silane chains on the catalysts features, we deeply investigated the surface properties by means of several physico-chemical characterization techniques and their relationship with the catalytic activity.

Table 1. Specific surface area (SSA), total pore volume (PV) and diol static contact angle (SCA) values

Sample	**SSA** / $m^2\ g^{-1}$	**Pore Volume** / $cm^3\ g^{-1}$	**SCA** (θ_{diol}) / °
SiO_2	410	0.63	50 ± 1
CuO/SiO_2	365	0.54	62 ± 1
CuO/SiO_2 – 1% TEOCS	358	0.52	65 ± 1
CuO/SiO_2 – 5% TEOCS	331	0.41	72 ± 1
CuO/SiO_2 – 10% TEOCS	245	0.37	75 ± 3
CuO/SiO_2– 15% TEOCS	263	0.50	75 ± 4

Firstly, specific surface area (SSA) and total pore volume (PV) of the samples were determined through nitrogen adsorption isotherms (see Table 1, 2nd and 3rd columns). The silane grafted samples possess slightly lower SSA and PV values than those of the bare catalyst (CuO/SiO_2). This phenomenon could be due to a progressive loss of accessibility of the pores due to the increasing alkylic chains interaction of the silane grafted catalysts.[44] The slightly increase of SSA

and PV in the case of the CuO/SiO_2 – 15% TEOCS could be due to the creation of a rougher surface due to the silane grafting.[51] The alkylic chain interactions of the organosilane residues will be discussed more deeply later in this paper.

To delve into the metallic phase surface morphology, TEM analyses were carried out on bare and silane coated samples. All the samples have similar morphologies; small copper nanoparticles (<2.3> nm, Figures 2 and Figure S1) appeared well dispersed onto the support. Neither aggregation nor copper nanoparticles (NPs) higher than 5 nm were detected (as showed in the size distribution diagrams, see Figure 2). A different scenario was observed for 15%-clad sample where copper nanoparticles are less detectable in TEM (Figure S1b) and pop up in STEM analysis (Figure S1b). Actually, HAADF-STEM (Figure S1b) contrast is proportional to the atomic number Z and it is less sensitive to the morphology, allowing the detection of buried particles in thin depth. Again, the nanoparticle size and sample morphology are, anyway, comparable to those of the other samples.

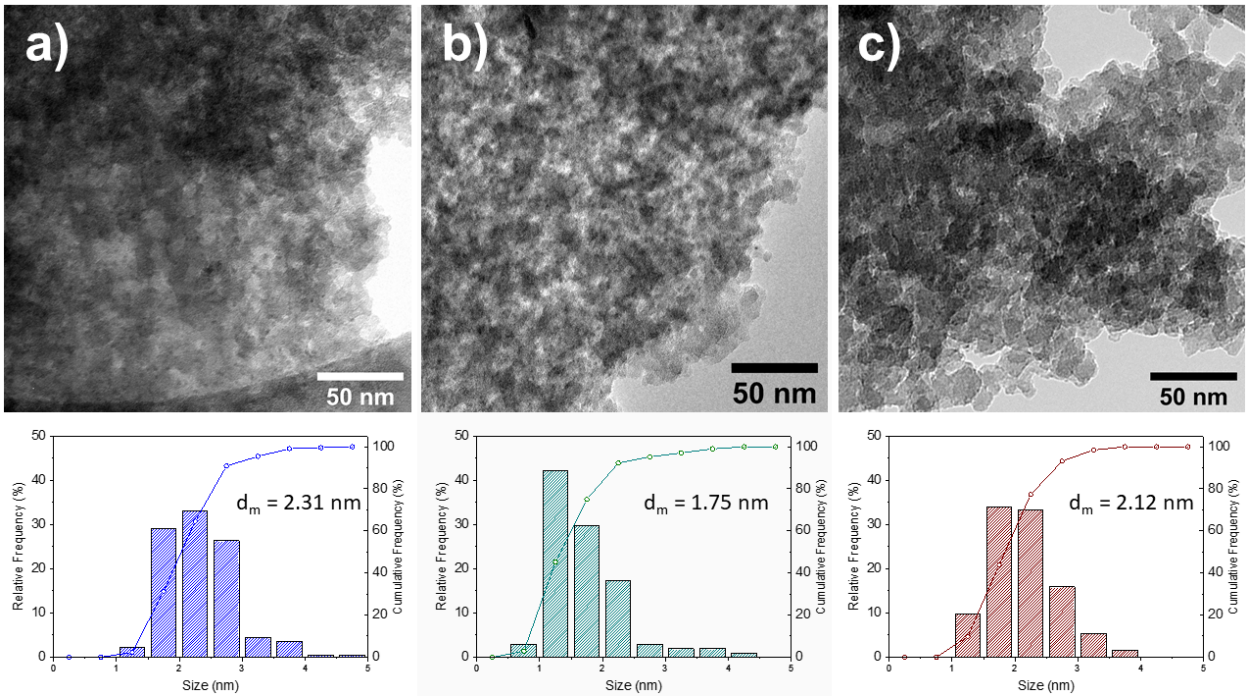

Figure 2. Representative TEM micrographs of selected samples a) CuO/SiO_2, b) CuO/SiO_2 - 5% TEOCS, c) CuO/SiO_2 - 10 % TEOCS, top, and associated size distributions of copper NPs, down.

The effective anchoring of octylsilane chains on the catalyst surface was confirmed by ATR spectroscopy and XPS spectroscopy (Figure 3). In ATR spectra the characteristic bands of alkanes were identified. In particular, the bands centered at 2926 cm^{-1} and 2853 cm^{-1} are respectively ascribable to the asymmetric and symmetric stretching of the C-H bond in the $-CH_2-$ moieties of the organosilane chains respectively. Moreover, the band at 2962 cm^{-1} is diagnostic of the asymmetric stretching of C-H bond in the $-CH_3$ groups.[35,52] The intensity of the alkane bands increases with the silane loading concentration coherently. The enrichment of silane groups at the catalyst surfaces was studied by XPS, also to investigate the influence of these groups on copper reducibility (Figure 3b and S2). Samples were analyzed before and after reduction (carried out as described in the Experimental Section). Notwithstanding the high complexity of the Si 2p and O 1s peaks do not allow an exhaustive fitting, only the main species can be identified (Figure 3b and S3a). The moderate enlargement of the Si and O bands is probably due to the appearance of contributions relative to the oxidation of the surface species[53] in our case represented by the siloxane bounds.

To prove the effective reduction of the copper centers even in the presence of the silane groups XPS analysis was performed on a selected sample (10% silane loading) investigating the copper state on the fresh calcined and the reduced catalyst surface. As it can be observed in Figure S2, Cu(II) species can be readily identified by Cu $2p^{3/2}$ peak at about 933 eV and of by Cu $2p^{1/2}$ peak at about 953 eV. It can be confirmed also acknowledging the presence of the typical shake up peaks near the main ones. The reduction of the copper phase was confirmed by the disappearance of the shake-up peak typical of the CuO species[54] and by the changing of the contribution peak areas.[49]

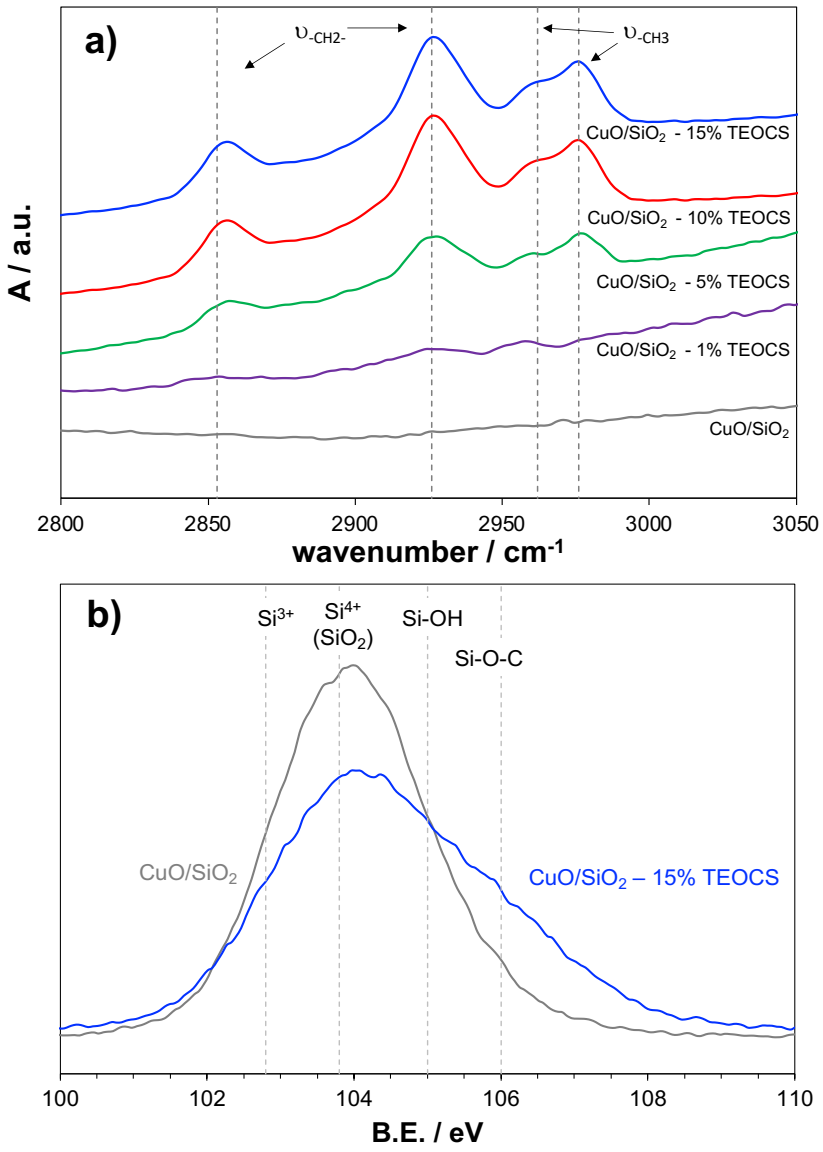

Figure 3. a) ATR spectra of the catalysts; b) XPS spectra, Si $2p^{3/2}$ band of bare sample CuO/SiO_2 and CuO/SiO_2 – 15% TEOCS. The typical bands of defective (Si^{3+})[55,56], $Si^{4+}(SiO_2)$[57,58], Si-OH[59], Si-O_3-C_3[60] are reported.

To ensure the stability of the silane chains under the reaction temperature, TG analyses were performed on the bare and silane modified samples. TG profiles are showed in Figure 4 while

onset and *end* temperature values of the two major weight loss events together with the associated weight loss percentages are reported in Table S1. The rank of mass loss evaluated at 550°C is the following: $Cu/SiO_2 \cong Cu/SiO_2 - 1\%$ TEOCS $<< Cu/SiO_2 - 5\%$ TEOCS $\cong Cu/SiO_2 - 10\%$ TEOCS $<< Cu/SiO_2 - 15\%$ TEOCS.

In general, physisorbed water loss is complete at around 200 °C, where a plateau is observed. Successively, another mass loss is observed around 320-330 °C, associated with the partial or total decomposition of the grafted silane.[48] As observed from the TG data, silane chains are stable onto the catalyst surface up to 320 °C, definitely compatible with the reaction conditions (160 °C).

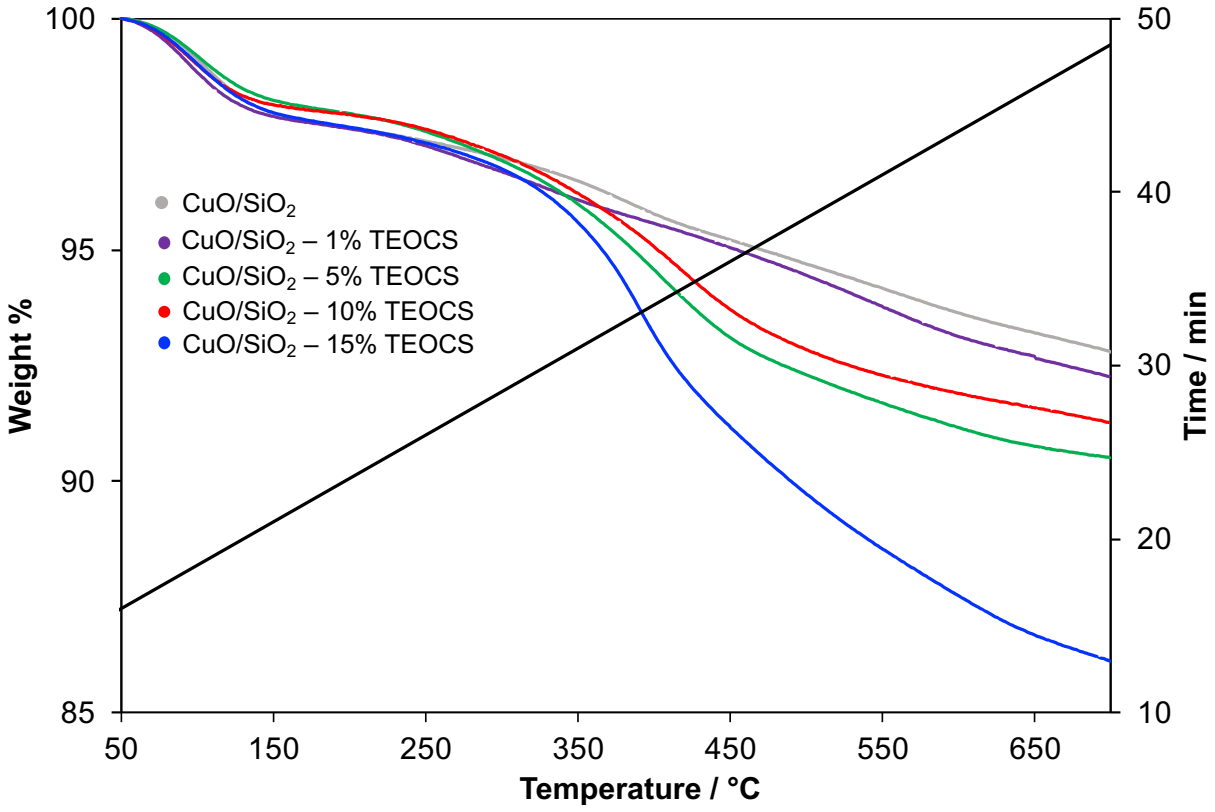

Figure 4. TGA profiles of all the CuO/SiO_2 samples

To have an insight into the wettability of the sample surfaces by varying silane loading,[61] the static contact angle (SCA) between the solid samples and 1,3-propandiol was measured (Table 1, 4th column). The 1,3-propandiol, being poorly viscous, was chosen to mimic the reaction product, *i.e.* 1,4-PDO, thus giving an overall idea of the alcoholphilicity of the surface. As it can be observed, copper deposition increases the SCA limiting the polarity of the surface due to the partial coverage of the surface hydroxyl groups of the silica. After the silane grafting, the surface affinity towards 1,3-propandiol decreases, passing from 62° of the bare catalyst to 75° of the CuO/SiO_2 - 15% TEOCS.

However, contact angle measurements possess some limitations due to the intrinsic porosity and surface roughness of the specimens. Hence, water adsorption isotherms represent a useful tool to assess the hydrophilicity of a porous solid giving a measure of its affinity to water.

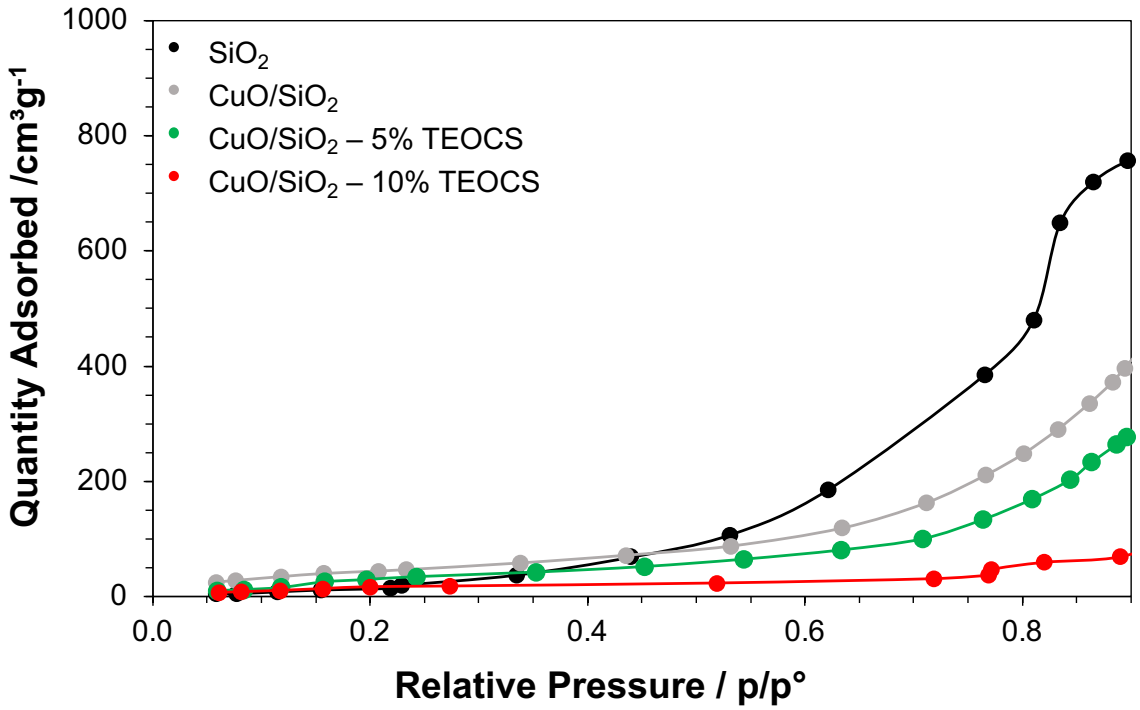

Figure 5. Water adsorption isotherms at temperature of 40°C on SiO_2, CuO/SiO_2, CuO/SiO_2 – 5% TEOCS and CuO/SiO_2 – 10 % TEOCS

The water adsorption capacity of the SiO_2 support and bare and functionalized CuO/SiO_2 catalysts is showed in Figure 5.

Also in this case, the same decreasing trend was observed already found in the N_2 adsorption experiments, *ie* the adsorption of water decreases as the density of the silane on CuO/SiO_2 increases.~~,~~ In particular, the computed monolayer volume, $V_{m,water}$, values pass from 42 cm^3/g to 22 cm^3/g for CuO/SiO_2 and CuO/SiO_2-10% TEOCS respectively (analogously to the decrease of $V_{m,N2}$ values computed for the N_2-adsorption experiments which diminish with the increase of silane loading passing from 84 to 29 cm^3/g for CuO/SiO_2 and CuO/SiO_2- 10% TEOCS respectively). As a consequence, some differences in SSA_{water} among samples are still appreciable passing from 128 m^2/g in the case of CuO/SiO_2 to 68 m^2/g in the case of the 10% silane loaded catalyst. This could be due to the hydrophobic interactions of the alkylic chains of the organosilanes that decreases the affinity of the surface towards water molecules.

Differences in the adsorbed water volume are more significant moving to higher relative pressures ($p/p° = 0.5$). The adsorbed volume of water decreases from silica to CuO/SiO_2 passing from 107.3 cm^3/g STP to 87.6 cm^3/g respectively and proportionally with the increase of silane surface density (from 87.6 cm^3/g for the bare catalyst going to 23.2 cm^3/g for the CuO/SiO_2- 10% TEOCS). These results corroborate the reduced surface polarity of the functionalized samples evaluated by contact angle measurements.

It is worth noting that a decrease of the overall hydrophilicity/polarity of the catalytic surface significantly improves the selectivity towards the 1,4-PDO (see Figure 1), preventing side reaction to occur, as showed also in our previous study.[49] On the other hand, the activity of the catalytic system remarkably decreases when the silane loading passes from 10% to 15% notwithstanding

the decrease of the alcoholphilicity decrease. In this respect, the different configuration of silane molecules bonded to the catalyst surface could play a role (Figure 6b) in masking the Cu sites.

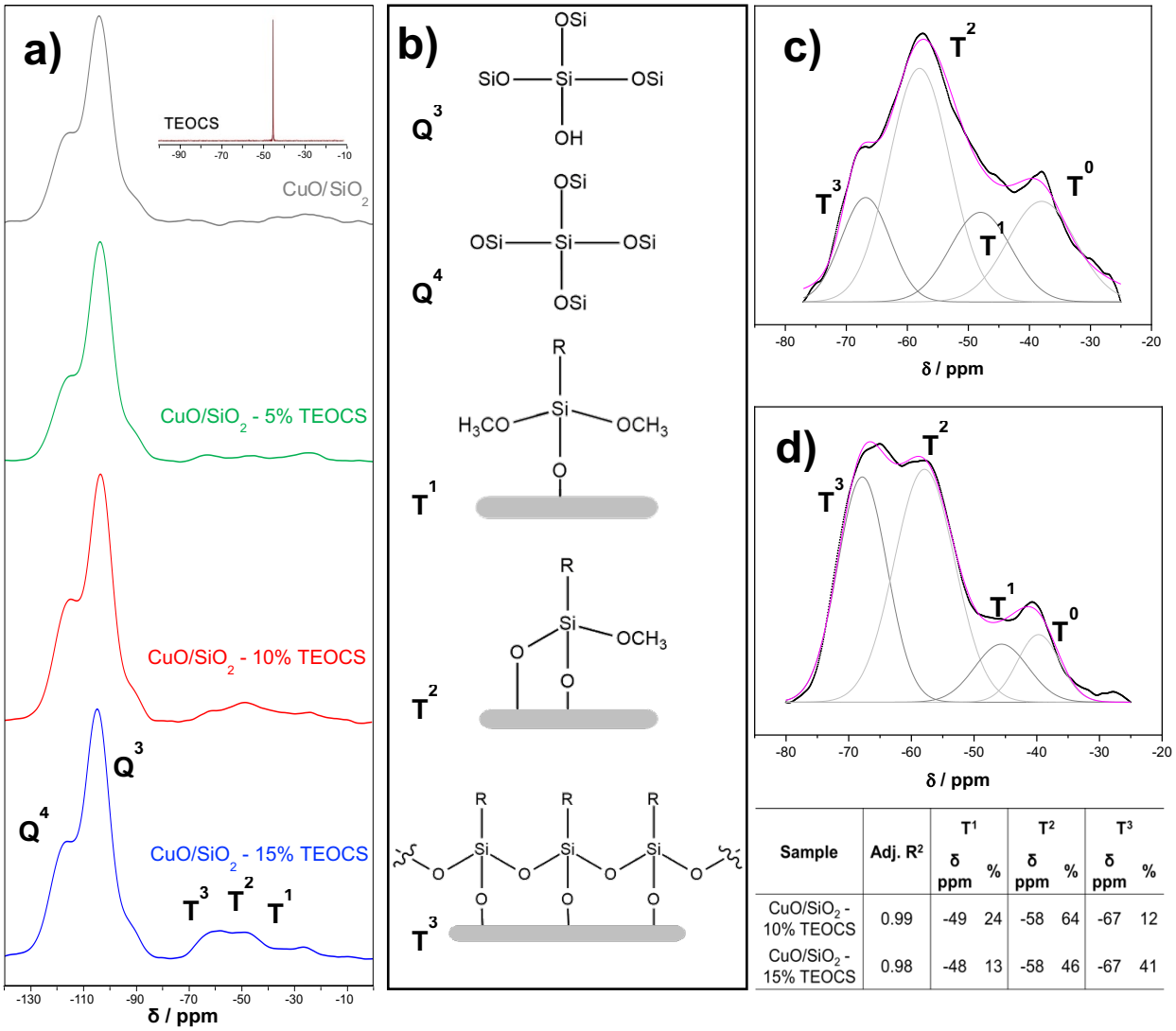

Sample	Adj. R^2	T^1 δ ppm	T^1 %	T^2 δ ppm	T^2 %	T^3 δ ppm	T^3 %
CuO/SiO_2 - 10% TEOCS	0.99	-49	24	-58	64	-67	12
CuO/SiO_2 - 15% TEOCS	0.98	-48	13	-58	46	-67	41

Figure 6. a) ^{29}Si NMR of pure triethylethoxysilane and ^{29}Si CP-MAS NMR of the sample catalysts; b) sketches of the possible silane/SiO_2 configurations; fitting procedures of c) CuO/SiO_2 – 10 % TEOCS and d) CuO/SiO_2 – 15 % TEOCS. Table: ^{29}Si CP-MAS NMR chemical shifts and relative percentages for the three proposed structures

Notably, TEOCS could be mainly grafted to the surface in three configurations: with a single bond (T^1), two bonds (T^2) and bonding with an adjacent silane chain (T^3).[44,62] According to this, the prevalence of a T^3 type structure could lead to a decrease in copper accessibility, hindering the GVL substrate to reach the hydrogenation active site. To confirm our hypothesis, ^{29}Si NMR of pure triethylethoxysilane as a standard and ^{29}Si CP-MAS NMR of the sample catalysts were performed. As displayed in Figure 6a inset, the $^{29}Si^1$-NMR pattern of TEOCS shows the presence of a singlet at -45 ppm. On the contrary, ^{29}Si CP-MAS of the bare CuO/SiO_2 present two important contributions ascribable to the bulky silica support: siloxane tetra-coordinate $Si–(OSi)_4$ (Q^4 at −110 pm), and bonded to a single silanol $Si–(OSi)_3–(OH)$ (Q^3 at −101 ppm).[63] Moreover, in the case of the functionalized catalysts, a second family of signals can be found at higher ppm, assigned to the organosilane bonds. Four distinguished contributions were found in the region between -80 and -30 ppm. Specifically, *i*) the contribution of the T^1 configuration was found at -49 ppm, *ii*) the signal at -58 ppm can be assigned to the T^2 structure, and finally *iii*) the contribution peak at -68 ppm could be ascribed to the T^3.[38,44,63] A small amount of the precursor (T^0) can still be found in the signal at -40 ppm.[64] In the case of CuO/SiO_2 -5% TEOCS, since the signal intensities are comparable to the background noise, no fitting analysis was performed. The comparison between CuO/SiO_2 -10% TEOCS and CuO/SiO_2 -15% TEOCS spectra reveals that the silane bounds in a different way according to its surface concentration. Specifically, we assist a decrease of both T^1 and T^2 bonding structures advantaging the T^3 in the 15% TEOCS sample (see the percentages of the peak deconvolutions in the Table inset in Figure 6. This indicates that the silane is prone to reticulate at higher concentration[44] limiting the copper site availability.

Copper nanoparticles of CuO/SiO_2 prepared with CH method, already showed a peculiar Lewis acidity when analyzed through FT-IR investigations after pyridine adsorption.[42] In this respect, the

use of probe molecules adsorption could shed some further light on copper accessibility as well as on knowledge of the nature of acid sites and total surface acidity.

With this scope, FT-IR spectra after pyridine adsorption on bare and functionalized catalysts were measured (Figure 7) and the concentration of their acid sites were evaluated (Table S2). This also allows one to investigate the possible influence of the silane on the acidity of the copper sites. All the samples maintain the acidity already observed on the catalyst prepared with CH method.[42] Furthermore, a more pronounced band at 1575 cm^{-1} was observed in the case of functionalized compounds. This could be probably due to the 8b mode of adsorbed pyridine corresponding to the vibrational modes of benzenic ring of pyridine.[65,66] As far as quantitative analysis is considered, the concentration of Lewis acid sites was higher for the silane-clad catalysts except for the 15% one. The moderate increase of acidity in the case of CuO/SiO_2 5% and 10% TEOCS suggests that TEOCS grafting plays a role in promoting the acidity of the surface. A plausible explanation could be searched in the mild electron withdrawing ability of Si: the possible formation of new -Cu-O-Si-R bonds could further lower the electron density of copper nanoparticles, enhancing their acidity. This was already observed in a work of Lin and co-workers[38] where silane grafting on copper phyllosilicates catalysts induced the formation of new acid sites. Surprisingly, the acidic site density of Cu/SiO_2 – 15% TEOCS catalyst drops to a value even lower with respect to that of the bare sample.

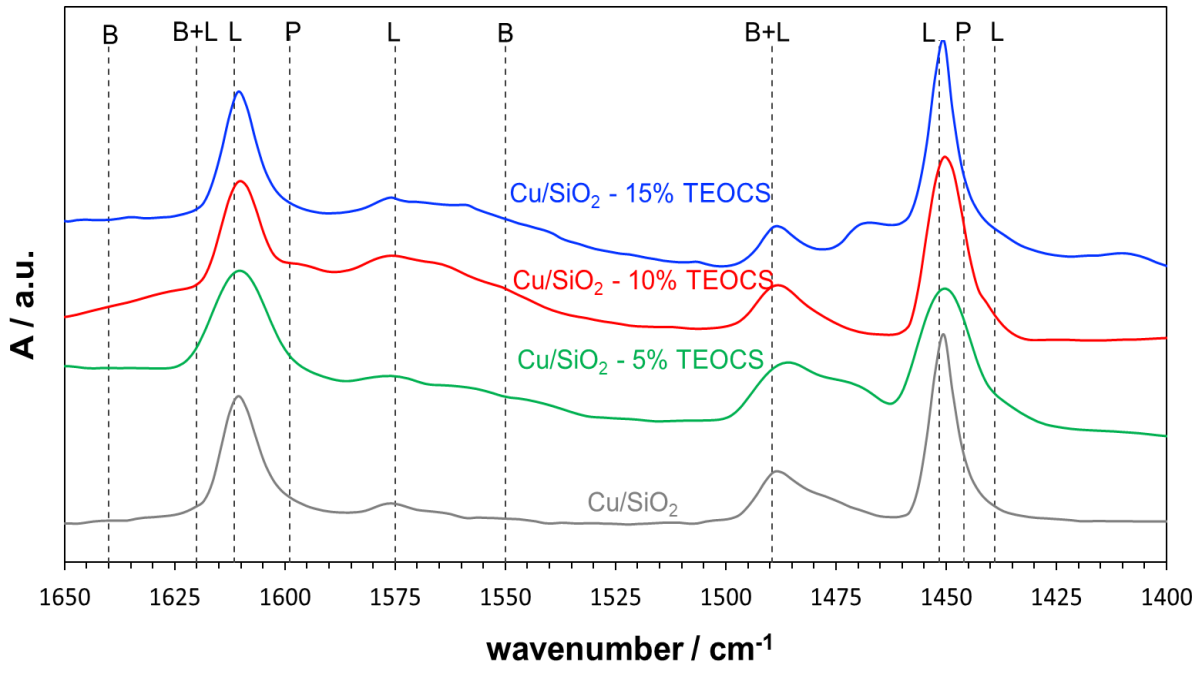

Figure 7. FT-IR spectra after pyridine adsorption of the catalysts (L = Lewis, B = Brønsted).

This could be clarified by the fact that a higher density of silane chains (as for the Cu/SiO_2 – 15% TEOCS) encourages the formation of more reticulated structures on the surface, as previously mentioned (^{29}Si CP MAS). This could hinder the pyridine probe to access the active sites thus supporting our hypothesis concerning the GVL interaction with Cu/SiO_2 – 15% TEOCS catalyst. This apparent reduction in acidity could be well due to a masking effect of the acidic sites by silane chains.

To measure the total surface acidity of the samples, gas-solid titrations of the acid sites were carried out using ammonia as probe. The results obtained by this method are reported in Table S2. Contrary to what was observed using pyridine, all of samples have comparable acidity (0.31-0.35 $mmol(NH_3)\ g_{cat}^{-1}$) demonstrating that copper sites maintained acid feature despite the silanization of the surface.

The reason of the different observed results by the use of pyridine or ammonia probes could be sought in the different steric hindrance of the two molecules. Ammonia has a much smaller kinetic diameter than pyridine, so it could be less affected by the steric hindering effect of silane chains and could titrate all the accessible Cu sites on sample surfaces independently of the silane density. Utilizing different probes with diverse size is often used as a method to assess accessibility of the acid sites.[66–69]

The information gained from the surface features such as morphology, wettability and acidity lead us to hypothesize a viable explanation of the critical aspects involved in the increased selectivity in the hydrogenation of GVL to 1,4-PDO. Wettability is a key factor in driving the removal of the diol product from the catalytic active sites. Notably, a lower hydrophilic/polar behavior of the catalyst surface by alkyl silane grafting allows a better desorption of the diol product, thus preventing dehydration side reactions. Actually, the selectivity towards the diol is increased up to 99% at the 5% w/w functionalization as soon as the silane easily reaches the surface. However, the great impact of acidity in the activation of GVL makes this aspect important in increasing conversion. This could explain the coherent trend of acidic sites density with GVL conversion with a maximum value (82%) obtained when working with of Cu/SiO_2 – 10% TEOCS catalyst and a significant decrease with Cu/SiO_2 – 15% TEOCS (0.34 against 0.22 $mmol_{py}\ g_{cat}^{-1}$ respectively). However, the activation of the substrate is directly connected to copper accessibility that appears to decrease with a too high TEOCS concentration (Figure 6). In this way, the proper choice with the anchoring degree of TEOCS allows to tune both the surface properties and the copper activity finding in the 10% loading the best trade-off for catalyst performances. The fine tuning of the surface grafting degree with hydrophobic residues is already known in the literature. The hydrophobization of Cu/ZnO catalyst showed a very positive inhibitory effect on the

unfavorable water–gas shift reaction in one-step synthesis of dimethyl ether from syngas keeping the catalytic activity very high. However, an excessing degree of stearic acid anchoring affected negatively the conversion due to a partial coverage of the active sites.[35]

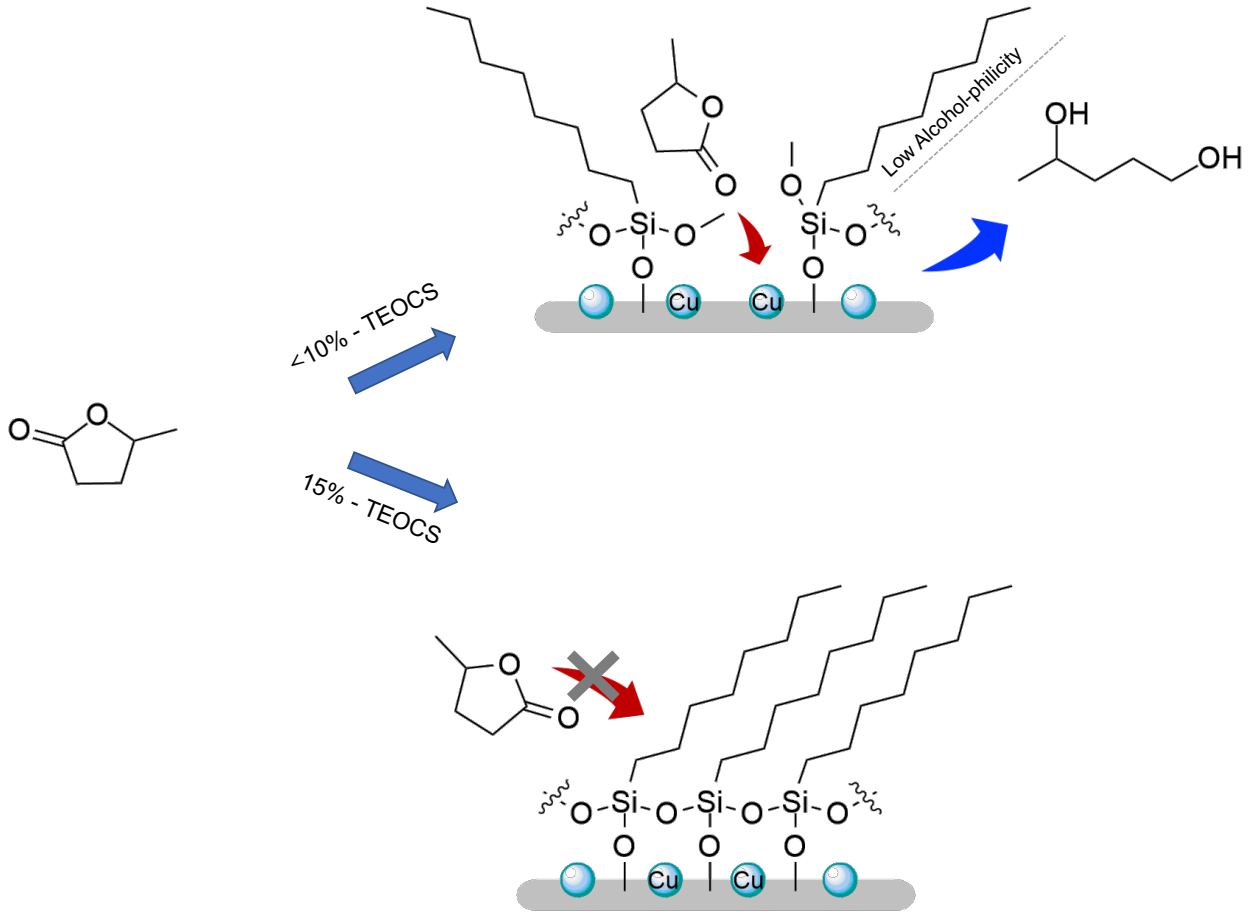

Figure 6. Possible mechanism for the hydrogenation of GVL on CuO/SiO_2 silane-grafted catalysts.

Conclusions

Biomass-derived platform molecules transformation requires particular attention in designing the properties of heterogeneous catalytic systems. In particular, the high oxygen content of biobased molecules entails a major role of their surface polarity. In this work we set up a simple

and reliable protocol for the surface modification of Cu/SiO_2 catalyst. The effective functionalization was confirmed by the appearance of alkanes bonds stretching signals (from ATR spectroscopy) together with new Si-O and O-C bands in XPS determinations. Then, these organosilane functionalized materials were tested in the hydrogenation of GVL to give 1,4-PDO. The results obtained clearly showed that the functionalization significantly lowers the alcoholphilicity of the surface (diol CA decrease of around 20%) resulting in an important increase in selectivity (20%) due to the easier desorption of the diol produced. Moreover, a huge reduction in water adsorption (around 75% at $p/p° = 0.5$) is appreciable for the sample covered by 10 % of the adopted silane molecule.

At the same time, this functionalization technique does not affect the copper phase activity. Actually, a silanization coverage up to 10% is desirable and leads to an increase in diol yield of about 40% reaching a selectivity of 98%, while a further organosilane loading gives rise to a decrease in activity due to the scarce accessibility of GVL to copper sites. This behavior is corroborated by CP MAS measurements showing a dense surface silane layer due to the presence of T^3 configuration. Hence, the capability to easily tune the wettability properties of the metal supported catalyst paves the way to a wide range of applications in which both the metallic phase activity and the polarity of the surface play a pivotal role in affecting the catalytic reaction.

AUTHOR INFORMATION

Corresponding Author*

Federica Zaccheria: CNR – SCITEC "G.Natta", via C. Golgi 19, 20133 Milano, email: federica.zaccheria@scitec.cnr.it

Giuseppe Cappelletti: Dipartimento di Chimica, Università degli Studi di Milano, via C. Golgi 19, 20133 Milano, email: giuseppe.cappelletti@unimi.it

Authors

Denise Cavuoto: Dipartimento di Chimica, Università degli Studi di Milano, via C. Golgi 19, 20133 Milano, CNR – SCITEC "G.Natta", via C. Golgi 19, 20133 Milano

Nicoletta Ravasio: CNR – SCITEC "G.Natta", via C. Golgi 19, 20133 Milano

Marcello Marelli: CNR – SCITEC "G.Natta", via G. Fantoli 16/15, I-20138 Milano

Sebastiano Campisi: Dipartimento di Chimica, Università degli Studi di Milano, via C. Golgi 19, 20133 Milano

Antonella Gervasini: Dipartimento di Chimica, Università degli Studi di Milano, via C. Golgi 19, 20133 Milano

Author Contributions

The manuscript was written through contributions of all authors. All authors have given approval to the final version of the manuscript.

ACKNOWLEDGMENT

The authors wish to thank the NMR facility of the Unitech COSPECT (Comprehensive Substances characterization via advanced sPECTtroscopy) at the University of Milan, where the NMR experiments have been performed

References

(1) Kubicka, D. Upgrading of Lipids to Hydrocarbon Fuels via (Hydro)Deoxygenation. *Chem*.

Catal. Biomass Upgrad. **2019**, 469–496. https://doi.org/10.1002/9783527814794.ch11.

(2) Gallezot, P. Conversion of Biomass to Selected Chemical Products. *Chemical Society Reviews*. 2012. https://doi.org/10.1039/c1cs15147a.

(3) Singhvi, M. S.; Gokhale, D. V. Lignocellulosic Biomass: Hurdles and Challenges in Its Valorization. *Appl. Microbiol. Biotechnol.* **2019**, *103* (23–24), 9305–9320. https://doi.org/10.1007/s00253-019-10212-7.

(4) Walker, T. W.; Motagamwala, A. H.; Dumesic, J. A.; Huber, G. W. Fundamental Catalytic Challenges to Design Improved Biomass Conversion Technologies. *J. Catal.* **2019**, *369*, 518–525. https://doi.org/10.1016/j.jcat.2018.11.028.

(5) Anchan, H. N.; Dutta, S. Recent Advances in the Production and Value Addition of Selected Hydrophobic Analogs of Biomass-Derived 5-(Hydroxymethyl)Furfural. *Biomass Convers. Biorefinery* **2021**. https://doi.org/10.1007/s13399-021-01315-1.

(6) Covinich, L. G.; Clauser, N. M.; Felissia, F. E.; Vallejos, M. E.; Area, M. C. The Challenge of Converting Biomass Polysaccharides into Levulinic Acid through Heterogeneous Catalytic Processes. *Biofuels, Bioprod. Biorefining* **2020**, *14* (2), 417–445. https://doi.org/10.1002/bbb.2062.

(7) Gayubo, A. G.; Aguayo, A. T.; Atutxa, A.; Aguado, R.; Bilbao, J. Transformation of Oxygenate Components of Biomass Pyrolysis Oil on a HZSM-5 Zeolite. I. Alcohols and Phenols. *Ind. Eng. Chem. Res.* **2004**, *43* (11), 2610–2618. https://doi.org/10.1021/ie030791o.

(8) Lee, A. F.; Wilson, K. Recent Developments in Heterogeneous Catalysis for the Sustainable Production of Biodiesel. *Catal. Today* **2015**, *242* (Part A), 3–18. https://doi.org/10.1016/j.cattod.2014.03.072.

(9) Kubička, D. Future Refining Catalysis - Introduction of Biomass Feedstocks. *Collect. Czechoslov. Chem. Commun.* **2008**, *73* (8–9), 1015–1044. https://doi.org/10.1135/cccc20081015.

(10) Sheldon, R. A.; Arends, I. W. C. E.; Hanefeld, U. *Green Chemistry and Catalysis*; 2007. https://doi.org/10.1002/9783527611003.

(11) Djakovitch, L.; Essayem, N.; Eternot, M.; Rataboul, F. A Landscape of Lignocellulosic Biopolymer Transformations into Valuable Molecules by Heterogeneous Catalysis in c'durable Team at Ircelyon. *Molecules* **2021**, *26* (22). https://doi.org/10.3390/molecules26226796.

(12) Cavuoto, D.; Zaccheria, F.; Ravasio, N. Some Critical Insights into the Synthesis and Applications of Hydrophobic Solid Catalysts. *Catalysts* **2020**, *10* (11), 1–26. https://doi.org/10.3390/catal10111337.

(13) Wang, L.; Xiao, F. S. The Importance of Catalyst Wettability. *ChemCatChem* **2014**, *6* (11), 3048–3052. https://doi.org/10.1002/cctc.201402437.

(14) Li, T.; Wang, J.; Wang, F.; Zhang, L.; Jiang, Y.; Arandiyan, H.; Li, H. The Effect of Surface Wettability and Coalescence Dynamics in Catalytic Performance and Catalyst Preparation: A Review. *ChemCatChem* **2019**, *11* (6), 1576–1586. https://doi.org/10.1002/cctc.201801925.

(15) Spanos, A. P.; Parulkar, A.; Brunelli, N. A. Enhancing Hydrophobicity and Catalytic Activity of Nano-Sn-Beta for Alcohol Ring Opening of Epoxides through Post-Synthetic Treatment with Fluoride. *J. Catal.* **2021**, *404*, 430–439. https://doi.org/10.1016/j.jcat.2021.10.023.

(16) Liu, F.; Huang, K.; Zheng, A.; Xiao, F. S.; Dai, S. Hydrophobic Solid Acids and Their Catalytic Applications in Green and Sustainable Chemistry. *ACS Catal.* **2018**, *8* (1), 372–391. https://doi.org/10.1021/acscatal.7b03369.

(17) Okuhara, T. Water-Tolerant Solid Acid Catalysts. *Chem. Rev.* **2002**, *102* (10), 3641–3666. https://doi.org/10.1021/cr0103569.

(18) Sánchez-Vázquez, R.; Pirez, C.; Iglesias, J.; Wilson, K.; Lee, A. F.; Melero, J. A. Zr-Containing Hybrid Organic-Inorganic Mesoporous Materials: Hydrophobic Acid Catalysts for Biodiesel Production. *ChemCatChem* **2013**, *5* (4), 994–1001. https://doi.org/10.1002/cctc.201200527.

(19) Manayil, J. C.; Lee, A. F.; Wilson, K. Functionalized Periodic Mesoporous Organosilicas: Tunable Hydrophobic Solid Acids for Biomass Conversion. *Molecules* **2019**, *24* (2). https://doi.org/10.3390/molecules24020239.

(20) Zhang, J.; Wang, L.; Liu, F.; Meng, X.; Mao, J.; Xiao, F. S. Enhanced Catalytic Performance in Dehydration of Sorbitol to Isosorbide over a Superhydrophobic Mesoporous Acid Catalyst. *Catal. Today* **2015**, *242* (PB), 249–254. https://doi.org/10.1016/j.cattod.2014.04.017.

(21) Cubo, A.; Iglesias, J.; Morales, G.; Melero, J. A.; Moreno, J.; Sánchez-Vázquez, R. Dehydration of Sorbitol to Isosorbide in Melted Phase with Propyl-Sulfonic Functionalized SBA-15: Influence of Catalyst Hydrophobization. *Appl. Catal. A Gen.* **2017**, *531* (5), 151–160. https://doi.org/10.1016/j.apcata.2016.10.029.

(22) Kong, P. S.; Pérès, Y.; Wan Daud, W. M. A.; Cognet, P.; Aroua, M. K. Esterification of Glycerol with Oleic Acid over Hydrophobic Zirconia-Silica Acid Catalyst and Commercial Acid Catalyst: Optimization and Influence of Catalyst Acidity. *Front. Chem.* **2019**, *7* (APR), 1–11. https://doi.org/10.3389/fchem.2019.00205.

(23) Kong, P. S.; Pérès, Y.; Cognet, P.; Senocq, F.; Daud, W. M. A. W.; Aroua, M. K.; Ahmad, H.; Sankaran, R.; Show, P. L. Structure–Selectivity Relationship of a Zirconia-Based Heterogeneous Acid Catalyst in the Production of Green Mono- and Dioleate Product. *Clean Technol. Environ. Policy* **2021**, *23* (1), 19–29. https://doi.org/10.1007/s10098-020-01830-1.

(24) Kong, P. S.; Cognet, P.; Pérès, Y.; Esvan, J.; Daud, W. M. A. W.; Aroua, M. K. Development of a Novel Hydrophobic ZrO2-SiO2 Based Acid Catalyst for Catalytic

Esterification of Glycerol with Oleic Acid. *Ind. Eng. Chem. Res.* **2018**, *57* (29), 9386–9399. https://doi.org/10.1021/acs.iecr.8b01609.

(25) Nguyen, V. C.; Bui, N. Q.; Mascunan, P.; Vu, T. T. H.; Fongarland, P.; Essayem, N. Esterification of Aqueous Lactic Acid Solutions with Ethanol Using Carbon Solid Acid Catalysts: Amberlyst 15, Sulfonated Pyrolyzed Wood and Graphene Oxide. *Appl. Catal. A Gen.* **2018**, *552* (November 2017), 184–191. https://doi.org/10.1016/j.apcata.2017.12.024.

(26) Sreeprasanth, P. S.; Srivastava, R.; Srinivas, D.; Ratnasamy, P. Hydrophobic, Solid Acid Catalysts for Production of Biofuels and Lubricants. *Appl. Catal. A Gen.* **2006**, *314* (2), 148–159. https://doi.org/10.1016/j.apcata.2006.08.012.

(27) Veiga, P. M.; Gomes, A. C. L.; Veloso, C. de O.; Henriques, C. A. Etherification of Different Glycols with Ethanol or 1-Octanol Catalyzed by Acid Zeolites. *Mol. Catal.* **2018**, *458*, 261–271. https://doi.org/10.1016/j.mcat.2017.10.027.

(28) Veiga, P. M.; Gomes, A. C. L.; Veloso, C. O.; Henriques, C. A. Acid Zeolites for Glycerol Etherification with Ethyl Alcohol: Catalytic Activity and Catalyst Properties. *Appl. Catal. A Gen.* **2017**, *548* (July), 2–15. https://doi.org/10.1016/j.apcata.2017.06.042.

(29) Losch, P.; Huang, W.; Vozniuk, O.; Goodman, E. D.; Schmidt, W.; Cargnello, M. Modular Pd/Zeolite Composites Demonstrating the Key Role of Support Hydrophobic/Hydrophilic Character in Methane Catalytic Combustion. *ACS Catal.* **2019**, *9* (6), 4742–4753. https://doi.org/10.1021/acscatal.9b00596.

(30) Silva, W. R.; Matsubara, E. Y.; Rosolen, J. M.; Donate, P. M.; Gunnella, R. Pd Catalysts Supported on Different Hydrophilic or Hydrophobic Carbonaceous Substrate for Furfural and 5-(Hydroxymethyl)-Furfural Hydrogenation in Water. *Mol. Catal.* **2021**, *504* (March). https://doi.org/10.1016/j.mcat.2021.111496.

(31) Wang, D.; Wang, S.; Jin, H.; Zhang, W.; Yang, Y.; Sun, A.; Tang, T.; Wang, J. Fabrication of Noble-Metal Catalysts with a Desired Surface Wettability and Their Applications in Deciphering Multiphase Reactions. *ACS Appl. Mater. Interfaces* **2013**, *5* (9), 3952–3958. https://doi.org/10.1021/am4006918.

(32) Mu, S.; Li, L.; Zhao, R.; Lu, H.; Dong, H.; Cui, C. Molecular-Scale Insights into Electrochemical Reduction of CO2on Hydrophobically Modified Cu Surfaces. *ACS Appl. Mater. Interfaces* **2021**, *13* (40), 47619–47628. https://doi.org/10.1021/acsami.1c13529.

(33) Wu, S.; Zhao, H.; Dong, F.; Ling, W.; Tang, Z.; Zhang, J. Construction of Superhydrophobic Ru/TiCeO Xcatalysts for the Enhanced Water Resistance of o-Dichlorobenzene Catalytic Combustion. *ACS Appl. Mater. Interfaces* **2021**, *13* (2), 2610–2621. https://doi.org/10.1021/acsami.0c18636.

(34) Hao, P.; Schwartz, D. K.; Medlin, J. W. Effect of Surface Hydrophobicity of Pd/Al2O3 on Vanillin Hydrodeoxygenation in a Water/Oil System. *ACS Catal.* **2018**, *8* (12), 11165–11173. https://doi.org/10.1021/acscatal.8b03141.

(35) Tan, M.; Tian, S.; Zhang, T.; Wang, K.; Xiao, L.; Liang, J.; Ma, Q.; Yang, G.; Tsubaki, N.;

Tan, Y. Probing Hydrophobization of a Cu/ZnO Catalyst for Suppression of Water-Gas Shift Reaction in Syngas Conversion. *ACS Catal*. **2021**, *11* (8), 4633–4643. https://doi.org/10.1021/acscatal.0c05585.

(36) Sheldon, R. A. Green and Sustainable Manufacture of Chemicals from Biomass: State of the Art. *Green Chem*. **2014**, *16* (3), 950–963. https://doi.org/10.1039/c3gc41935e.

(37) Stadler, B. M.; Brandt, A.; Kux, A.; Beck, H.; de Vries, J. G. Properties of Novel Polyesters Made from Renewable 1,4-Pentanediol. *ChemSusChem* **2020**, *13* (3), 556–563. https://doi.org/10.1002/cssc.201902988.

(38) Tsou, Y. J.; To, T. D.; Chiang, Y. C.; Lee, J. F.; Kumar, R.; Chung, P. W.; Lin, Y. C. Hydrophobic Copper Catalysts Derived from Copper Phyllosilicates in the Hydrogenation of Levulinic Acid to γ-Valerolactone. *ACS Appl. Mater. Interfaces* **2020**, *12* (49), 54851–54861. https://doi.org/10.1021/acsami.0c17612.

(39) Yismaw, S.; Ebbinghaus, S. G.; Wenzel, M.; Poppitz, D.; Gläser, R.; Matysik, J.; Bauer, F.; Enke, D. Selective Functionalization of the Outer Surface of MCM-48-Type Mesoporous Silica Nanoparticles at Room Temperature. *J. Nanoparticle Res*. **2020**, *22* (9). https://doi.org/10.1007/s11051-020-05006-2.

(40) Bauer, F.; Meyer, R.; Bertmer, M.; Naumov, S.; Al-Naji, M.; Wissel, J.; Steinhart, M.; Enke, D. Silanization of Siliceous Materials, Part 3: Modification of Surface Energy and Acid-Base Properties of Silica Nanoparticles Determined by Inverse Gas Chromatography (IGC). *Colloids Surfaces A Physicochem. Eng. Asp*. **2021**, *618* (March), 126472. https://doi.org/10.1016/j.colsurfa.2021.126472.

(41) Kim, H. J.; Brunelli, N. A.; Brown, A. J.; Jang, K. S.; Kim, W. G.; Rashidi, F.; Johnson, J. R.; Koros, W. J.; Jones, C. W.; Nair, S. Silylated Mesoporous Silica Membranes on Polymeric Hollow Fiber Supports: Synthesis and Permeation Properties. *ACS Appl. Mater. Interfaces* **2014**, *6* (20), 17877–17886. https://doi.org/10.1021/am504581j.

(42) Zaccheria, F.; Scotti, N.; Marelli, M.; Psaro, R.; Ravasio, N. Unravelling the Properties of Supported Copper Oxide: Can the Particle Size Induce Acidic Behaviour? *Dalt. Trans*. **2013**, *42* (5), 1319–1328. https://doi.org/10.1039/c2dt32454g.

(43) Scotti, N.; Dangate, M.; Gervasini, A.; Evangelisti, C.; Ravasio, N.; Zaccheria, F. Unraveling the Role of Low Coordination Sites in a Cu Metal Nanoparticle: A Step toward the Selective Synthesis of Second Generation Biofuels. *ACS Catal*. **2014**, *4* (8), 2818–2826. https://doi.org/10.1021/cs500581a.

(44) Milanesi, F.; Cappelletti, G.; Annunziata, R.; Bianchi, C. L.; Meroni, D.; Ardizzone, S. Siloxane-TiO2 Hybrid Nanocomposites. the Structure of the Hydrophobic Layer. *J. Phys. Chem. C* **2010**, *114* (18), 8287–8293. https://doi.org/10.1021/jp1014669.

(45) Meroni, D.; Ardizzone, S.; Cappelletti, G.; Ceotto, M.; Ratti, M.; Annunziata, R.; Benaglia, M.; Raimondi, L. Interplay between Chemistry and Texture in Hydrophobic TiO2 Hybrids. *J. Phys. Chem. C* **2011**, *115* (38), 18649–18658. https://doi.org/10.1021/jp205142b.

(46) Emeis, C. A. Determination of Integrated Molar Extinction Coefficients for Infrared Absorption Bands of Pyridine Adsorbed on Solid Acid Catalysts. *Journal of Catalysis*. 1993, pp 347–354. https://doi.org/10.1006/jcat.1993.1145.

(47) Campisi, S.; Galloni, M. G.; Marchetti, S. G.; Auroux, A.; Postole, G.; Gervasini, A. Functionalized Iron Hydroxyapatite as Eco-Friendly Catalyst for NH3-SCR Reaction: Activity and Role of Iron Speciation on the Surface. *ChemCatChem* **2020**, *12* (6), 1676–1690. https://doi.org/10.1002/cctc.201901813.

(48) Castellano, M.; Marsano, E.; Turturro, A.; Conzatti, L.; Busca, G. Dependence of Surface Properties of Silylated Silica on the Length of Silane Arms. *Adsorption* **2012**, *18* (3–4), 307–320. https://doi.org/10.1007/s10450-012-9402-6.

(49) Cavuoto, D.; Ravasio, N.; Scotti, N.; Gervasini, A.; Campisi, S.; Marelli, M.; Cappelletti, G.; Zaccheria, F. A Green Solvent Diverts the Hydrogenation of γ – Valerolactone to 1 , 4 - Pentandiol over Cu / SiO 2. *Mol. Catal.* **2021**, *516* (September), 111936. https://doi.org/10.1016/j.mcat.2021.111936.

(50) Du, X. L.; Bi, Q. Y.; Liu, Y. M.; Cao, Y.; He, H. Y.; Fan, K. N. Tunable Copper-Catalyzed Chemoselective Hydrogenolysis of Biomass-Derived γ-Valerolactone into 1,4-Pentanediol or 2-Methyltetrahydrofuran. *Green Chem.* **2012**, *14* (4), 935–939. https://doi.org/10.1039/c2gc16599f.

(51) Rytter, E.; Salman, A. ul R.; Tsakoumis, N. E.; Myrstad, R.; Yang, J.; Lögdberg, S.; Holmen, A.; Rønning, M. Hydrophobic Catalyst Support Surfaces by Silylation of Γ-Alumina for Co/Re Fischer-Tropsch Synthesis. *Catal. Today* **2018**, *299* (May 2017), 20–27. https://doi.org/10.1016/j.cattod.2017.04.031.

(52) Silverstein, R. M.; Webster, F. X.; Kiemle, D. J.; Bryce, D. L. *Spectrometric Identification of Organic Compounds*, 8th Editio.; John Wiley & Sons, Inc., 2014.

(53) Alam, A. U.; Howlader, M. M. R.; Deen, M. J. Oxygen Plasma and Humidity Dependent Surface Analysis of Silicon, Silicon Dioxide and Glass for Direct Wafer Bonding. *ECS J. Solid State Sci. Technol.* **2013**, *2* (12), P515–P523. https://doi.org/10.1149/2.007312jss.

(54) Biesinger, M. C. Advanced Analysis of Copper X-Ray Photoelectron Spectra. *Surf. Interface Anal.* **2017**, *49* (13), 1325–1334. https://doi.org/10.1002/sia.6239.

(55) Ma, J. W.; Lee, W. J.; Bae, J. M.; Jeong, K. S.; Oh, S. H.; Kim, J. H.; Kim, S. H.; Seo, J. H.; Ahn, J. P.; Kim, H.; et al. Carrier Mobility Enhancement of Tensile Strained Si and SiGe Nanowires via Surface Defect Engineering. *Nano Lett.* **2015**, *15* (11), 7204–7210. https://doi.org/10.1021/acs.nanolett.5b01634.

(56) Kitao, A.; Imakita, K.; Kawamura, I.; Fujii, M. An Investigation into Second Harmonic Generation by Si-Rich SiNx Thin Films Deposited by RF Sputtering over a Wide Range of Si Concentrations. *J. Phys. D. Appl. Phys.* **2014**, *47* (21). https://doi.org/10.1088/0022-3727/47/21/215101.

(57) Pargoletti, E.; Verga, S.; Chiarello, G. L.; Longhi, M.; Cerrato, G.; Giordana, A.;

Cappelletti, G. Exploring SNx Ti1−x O2 Solid Solutions Grown onto Graphene Oxide (GO) as Selective Toluene Gas Sensors. *Nanomaterials* **2020**, *10* (4). https://doi.org/10.3390/nano10040761.

(58) Dietrich, P. M.; Glamsch, S.; Ehlert, C.; Lippitz, A.; Kulak, N.; Unger, W. E. S. Synchrotron-Radiation XPS Analysis of Ultra-Thin Silane Films: Specifying the Organic Silicon. *Appl. Surf. Sci.* **2016**, *363*, 406–411. https://doi.org/10.1016/j.apsusc.2015.12.052.

(59) Post, P.; Wurlitzer, L.; Maus-Friedrichs, W.; Weber, A. P. Characterization and Applications of Nanoparticles Modified In-Flight with Silica or Silica-Organic Coatings. *Nanomaterials* **2018**, *8* (7), 1–19. https://doi.org/10.3390/nano8070530.

(60) Su, D.; Wang, L.; Liang, K.; Zhang, F.; Lin, D.; Hu, Y.; Ji, H.; Li, X.; Chen, S.; Yan, X. Silicon Oxycarbide/Titanium Dioxide Fibers with Wrinkle-like Surface by Electrospinning. *Mater. Lett.* **2016**, *172*, 202–206. https://doi.org/10.1016/j.matlet.2016.02.150.

(61) Soliveri, G.; Annunziata, R.; Ardizzone, S.; Cappelletti, G.; Meroni, D. Multiscale Rough Titania Films with Patterned Hydrophobic/Oleophobic Features. *J. Phys. Chem. C* **2012**, *116* (50), 26405–26413. https://doi.org/10.1021/jp309397c.

(62) Protsak, I. S.; Morozov, Y. M.; Dong, W.; Le, Z.; Zhang, D.; Henderson, I. M. A 29Si, 1H, and 13C Solid-State NMR Study on the Surface Species of Various Depolymerized Organosiloxanes at Silica Surface. *Nanoscale Res. Lett.* **2019**, *14*. https://doi.org/10.1186/s11671-019-2982-2.

(63) Bui, T. V.; Umbarila, S. J.; Wang, B.; Sooknoi, T.; Li, G.; Chen, B.; Resasco, D. E. High-Temperature Grafting Silylation for Minimizing Leaching of Acid Functionality from Hydrophobic Mesoporous Silicas Used as Catalysts in the Liquid Phase. *Langmuir* **2019**, *35* (21), 6838–6852. https://doi.org/10.1021/acs.langmuir.9b00487.

(64) Nam, K. H.; Lee, T. H.; Bae, B. S.; Popall, M. Condensation Reaction of 3-(Methacryloxypropyl)-Trimethoxysilane and Diisobutylsilanediol in Non-Hydrolytic Sol-Gel Process. *J. Sol-Gel Sci. Technol.* **2006**, *39* (3), 255–260. https://doi.org/10.1007/s10971-006-7884-y.

(65) Escribano, V. S.; del Hoyo Martínez, C.; Fernández López, E.; Gallardo Amores, J. M.; Busca, G. Characterization of a Ceria-Zirconia-Supported Cu Oxides Catalyst: An FT-IR Study on the Catalytic Oxidation of Propylene. *Catal. Commun.* **2009**, *10* (6), 861–864. https://doi.org/10.1016/j.catcom.2008.12.024.

(66) Busca, G. Spectroscopic Characterization of the Acid Properties of Metal Oxide Catalysts. *Catal. Today* **1998**, *41* (1–3), 191–206. https://doi.org/10.1016/S0920-5861(98)00049-2.

(67) Freitas, C.; Barrow, N. S.; Zholobenko, V. Accessibility and Location of Acid Sites in Zeolites as Probed by Fourier Transform Infrared Spectroscopy and Magic Angle Spinning Nuclear Magnetic Resonance. *Johnson Matthey Technol. Rev.* **2018**, *62* (3), 279–290. https://doi.org/10.1595/205651318X696792.

(68) Busca, G.; Gervasini, A. *Solid Acids, Surface Acidity and Heterogeneous Acid Catalysis*,

1st ed.; Elsevier Inc., 2020; Vol. 67. https://doi.org/10.1016/bs.acat.2020.09.003.

(69) Nguyen, V. C.; Kheireddine, S.; Dandach, A.; Eternot, M.; Vu, T. T. H.; Essayem, N. Acid Properties of GO and Reduced GO as Determined by Microcalorimetry, FTIR, and Kinetics of Cellulose Hydrolysis-Hydrogenolysis. *Catalysts* **2020**, *10* (12), 1–13. https://doi.org/10.3390/catal10121393.